



n-Heptane/air combustion in perfectly stirred reactors: Dynamics, bifurcations and dominant reactions at critical conditions



Mahdi Kooshkbaghi, Christos E. Frouzakis*, Konstantinos Boulouchos, Iliya V. Karlin

Aerothermochemistry and Combustion Systems Laboratory, Swiss Federal Institute of Technology, Zurich CH-8092, Switzerland

ARTICLE INFO

Article history:

Received 9 April 2015

Received in revised form 4 May 2015

Accepted 4 May 2015

Available online 10 June 2015

Keywords:

n-heptane kinetics

Numerical continuation and bifurcation analysis

Bogdanov–Takens bifurcation

Cusp bifurcation

Computational singular perturbation

Entropy production analysis

ABSTRACT

The dynamics of *n*-heptane/air mixtures in perfectly stirred reactors (PSR) is investigated systematically using bifurcation and stability analysis and time integration. A skeletal mechanism of *n*-heptane constructed by entropy production analysis is employed, which is extensively validated for different conditions with respect to the ignition delay time, laminar flame speed, and the typical hysteretic behavior observed in PSRs. The significantly reduced size of the skeletal mechanism, enables the extension of the bifurcation analysis to multiple parameters. In addition to residence time, the effect of equivalence ratio, volumetric heat loss and the simultaneous variation of residence time and inlet temperature on the reactor state are investigated using one- and two-parameter continuations. Multiple ignition and extinction turning points leading to steady state multiplicity and oscillatory behavior of both the strongly burning and the cool flames are found, which can lead to oscillatory (dynamic) extinction. The two-parameter continuations revealed isolas and codimension-two bifurcations (cusp, Bogdanov–Takens, and double Hopf). Computational Singular Perturbation (CSP) and entropy production analysis were used to probe the complex kinetics at interesting points of the bifurcation diagrams.

© 2015 The Combustion Institute. Published by Elsevier Inc. All rights reserved.

1. Introduction

The Perfectly Stirred Reactor (PSR) or Continuous Stirred Tank Reactor (CSTR) is commonly used to study complex chemical kinetics and combustion dynamics. In practice, such reactors can be realized by intense mixing using gas reactant jets in a jet-stirred reactor [1]. Efficient mixing provides homogeneous conditions so that the state at the reactor exit is the same as inside, simplifying strongly its numerical modeling.

Since the rigorous analysis of Bilous and Amundson in 1955 [2] and the more comprehensive numerical study of Aris and Amundson [3], the reactor dynamics and stability for the single-step irreversible exothermic reaction $R \rightarrow P$ have been investigated extensively, revealing interesting dynamics which include multiple equilibria and hysteresis loops, super- and subcritical Hopf bifurcations, and complex oscillations (see, for example, [4–6]).

The dependence of the reactor state (indicated for example by its temperature T) on τ , the residence time in the reactor, typically

displays an S-shaped curve, connecting the weakly- and strongly burning steady state branches via an unstable steady state branch between the ignition and extinction points [7]. The lower branch of the bifurcation diagram that shows the possible long-term states drawn schematically in Fig. 1 starts from the chemically frozen state at very short residence time and remains weakly reacting up to the residence time of ignition τ_{ign} , where the system state jumps to the strongly burning branch. Starting from a state on the latter branch, the gradual decrease of τ will eventually lead the reactor back to the weakly reacting state at τ_{ext} , the residence time of extinction. Steady state multiplicity exists for $\tau_{ext} \leq \tau \leq \tau_{ign}$, and the reactor operation becomes sensitive to external perturbations.

More complete pictures of the qualitative features of PSRs and phase portraits for various scenarios of bifurcation diagram have been obtained analytically and numerically for single-step reactions and lumped variables [8–10]. PSRs have also been investigated via Lyapunov's direct method [11], parametric sensitivity [12] as well as from the control and stabilization point of view (e.g. [13]). A discussion of earlier theoretical and experimental studies of ignition and cool flames in CSTRs can be found in the review of Griffiths and Scott [14], the book [6] and the references therein. The ignition and extinction conditions are used for the

* Corresponding author at: Aerothermochemistry and Combustion Systems Laboratory, Swiss Federal Institute of Technology (ETH), Sonneggstrasse 3, Zurich CH-8092, Switzerland.

E-mail address: frouzakis@lav.mavt.ethz.ch (C.E. Frouzakis).

validation and rate constant tuning of detailed and reduced mechanisms by comparison with experimental data (see, for example, [15]).

Although the dynamic behavior of PSRs using generic single- or few-steps reactions has been systematically analyzed, few literature studies have considered detailed reaction mechanisms. Numerical investigations of hydrogen combustion in isothermal PSRs [16–18] revealed complex dynamics which in addition to ignitions and extinctions included oscillations and birhythmicity (coexistence of two stable limit cycles for the same operating conditions). Sensitivity and principal component analysis at the bifurcation points were used to construct minimal reaction mechanisms that can predict state multiplicity [17]. Recent investigations of ignition/extinction behavior of more complex fuels like dimethyl ether [19,20] and *n*-heptane [21] in PSRs focused on the detection of important features with respect to the variation of a single parameter (the residence time) and its effect on the type of extinction (sudden jump to the weakly burning or extinguished state or dynamic extinction via oscillations of increasing amplitude) [20].

The complexity of the reaction mechanism in terms of the number of species and reactions increases dramatically with the size of the fuel molecule [22], and even for ideal homogeneous reactors like the PSR the computational cost becomes high, particularly when a large number of parameters determines the behavior. Thanks to the availability of efficient numerical continuation packages, the analysis of the dynamics of single- or few-steps global reactions can be expanded to detailed mechanisms including hundreds of species and thousands of elementary reactions. The efficient scanning of the dynamics with respect to multiple operating parameters can identify the critical conditions leading to the transition between different reactor states and provide essential information not only to enhance our understanding of the phenomenology of combustion chemistry, but also for the design of experiments to probe different types of kinetics for mechanism validation purposes.

In the present study, we employ a skeletal mechanism constructed using the recently proposed reduction approach that is based on the relative contribution of elementary reactions to the total entropy production [23]. Comparisons with the detailed scheme show that the skeletal mechanism reproduces accurately not only the ignition delay and the laminar flame speed over a wide range of conditions, but it can also accurately capture the complex PSR dynamics including the bifurcation points.

The bifurcation diagram summarizing the possible dynamics as well as the transitions leading from one state to another can be generated by finding the long-time state for the system of equations describing the dynamics for different values of the controlling parameter(s). In a brute force manner, this can be achieved by scanning the parameter space and numerically integrating the transient equations modeling the temporal evolution of the concentration and temperature in the reactor (Section 2) starting from different initial conditions. The dynamics in a PSR is determined by five parameters: the residence time τ , inlet temperature T_0 , pressure p , equivalence ratio ϕ and heat loss per unit volume \dot{Q}_{loss} , and the brute force method becomes impractical. In addition to the excessive number of integrations that are required, this approach can only identify stable steady or oscillatory states.

Arc-length continuation methods [24] offer an accurate and more efficient way to track changes in the long-term behavior by starting from a particular solution and following it as one or more parameters are varied. Unstable solutions can be computed, and the local stability can be determined by the eigenvalues of the Jacobian matrix obtained by linearization of the governing equations around the desired state: eigenvalues with negative (positive) real parts define stable (unstable) states. In this work,

the AUTO-07p package [25,26] is employed to systematically follow the transitions in the observed behavior, first with respect to independent variations of τ and \dot{Q}_{loss} for fixed values of the remaining parameters (one-parameter continuations), and then for the simultaneous variation of τ and T_0 (two-parameter continuation). The effect of equivalence ratio and pressure is assessed by computing the two-parameter diagrams for different values of ϕ and p to partially construct three-parameter diagrams. The observed dynamics include steady and oscillatory strongly burning states and cool flames, multistability over extended ranges of operating conditions and higher codimension bifurcations.

Entropy production analysis can also provide useful information about elementary reactions responsible for bringing the system state to equilibrium. Computational Singular Perturbation (CSP) analysis is also employed to identify the dominant reactions at the bifurcation points. CSP is a time-scale based approach that has been used for the identification of slow and fast processes (e.g. [27]), skeletal and reduced mechanism generation (e.g. [28,29]), analysis of two-stage *n*-heptane ignition [30], as well as flow-chemistry interactions in limiting phenomena [31,32]. The CSP analysis is performed on the so-called explosive mode, i.e. the mode with time scale corresponding to the positive or the least negative eigenvalue of the Jacobian matrix at the state of interest. The corresponding eigenvector, a first-order approximation to the CSP mode, is used to identify the most important reactions at extinction, ignition or oscillatory combustion with the help of the amplitude [33] and time scale participation [34] indices. More detailed CSP-based analyses of autoignition and the multi-stage ignition of *n*-heptane can be found in [35,30,36].

The work presented here is along the lines of the work of Lu and co-workers who studied combustion dynamics in PSRs for *n*-heptane [21], methane [19] and DME [19,20]. One-parameter continuations with respect to the residence time were performed in these works focusing on ignition and extinction, and a variant of the CSP method, the Chemical Explosive Mode Analysis (CEMA) [37], was used to analyze the kinetics.

The paper is organized as follows: Following the presentation of the PSR governing equations in Section 2 and a brief discussion of numerical continuation in Section 3, the skeletal mechanism that was generated using entropy production analysis is presented in Section 4. The CSP analysis tools used are briefly reviewed in Section 5, before turning to the results of numerical calculations both from the chemical kinetics and the dynamical system points of view (Section 6).

2. Governing equations

A system of n_s chemical species M_i , $i = 1, \dots, n_s$ is considered, which reacts according to a mechanism of n_r reversible elementary reactions

$$\sum_{i=1}^{n_s} \nu'_{ik} M_i \rightleftharpoons \sum_{i=1}^{n_s} \nu''_{ik} M_i, \quad k = 1, \dots, n_r \quad (1)$$

Stoichiometry is defined by ν'_{ik} and ν''_{ik} , the stoichiometric coefficients of species i in reaction k for the reactants and products, respectively. The rate of the elementary reaction k is

$$q_k = q_k^f - q_k^r = k_k^f \prod_{i=1}^{n_s} [X_i]^{\nu'_{ik}} - k_k^r \prod_{i=1}^{n_s} [X_i]^{\nu''_{ik}} \quad k = 1, \dots, n_r \quad (2)$$

where $[X_i]$ denotes molar concentration of species i and k_k^f and k_k^r are the forward and reverse rate constants of reaction k . The production/consumption rate of the i th species $\dot{\omega}_i$ is the summation of the rates of all reactions involving the species i

$$\dot{\omega}_i = \sum_{k=1}^{n_r} v_{ik} q_k \quad (3)$$

where $v_{ik} = v''_{ik} - v'_{ik}$ is the net stoichiometric coefficient.

The temporal evolution of Y_i , the mass fraction of species i , and temperature T in a perfectly stirred reactor is described by a system of ordinary differential equations (ODEs)

$$\frac{dY_i}{dt} = \frac{1}{\tau} (Y_i^0 - Y_i) + \frac{\dot{\omega}_i W_i}{\rho} \quad i = 1, \dots, n_s \quad (4)$$

$$\frac{dT}{dt} = \frac{1}{c_p \tau} \sum_{i=1}^{n_s} (h_i^0 - h_i) Y_i - \frac{1}{\rho c_p} \sum_{i=1}^{n_s} h_i W_i \dot{\omega}_i - \frac{\dot{Q}_{loss}}{\rho c_p}$$

where Y_i^0 and h_i^0 are the mass fraction and total enthalpy of species i at the inflow with temperature T_0 , W_i and h_i the molecular weight and total enthalpy of species i , \bar{c}_p and ρ the mixture heat capacity under constant pressure and density, and \dot{Q}_{loss} the heat loss per unit volume. With the equivalence ratio ϕ defining the inlet composition Y_i^0 , the system state is described by the $n_s + 1$ dimensional vector $\mathbf{z} = [Y_i, T]$, $i = 1, \dots, n_s$ for specified values of the components of the five-dimensional parameter vector $\Gamma = [\tau, \phi, T_0, p, \dot{Q}_{loss}]$; p is the reactor pressure.

Starting from an initial condition $\mathbf{z} = \mathbf{z}(t = 0)$, the initial value problem (4) can be integrated for specified values of the parameters using the stiff ordinary differential equation solver DVODE [38] to compute the temporal evolution of the reactor state. The chemical source term and the thermodynamic properties are computed using CHEMKIN [39]. At long times the system evolves towards either a steady (equilibrium) or an oscillatory state (limit cycle or periodic orbit). In general, bounded solutions of systems of autonomous ODEs can also converge at long times to more complex attractors, like tori (quasi-periodic orbits) or strange attractors (chaotic orbits) (for example, see [40,41]).

3. Numerical bifurcation analysis

Time integration can be used to explore the dynamics in a brute-force way for different combinations of parameters and initial conditions. In the general case, slight changes of the parameters result in small changes of the long-term dynamics, and the dynamical system displays structural stability. However, at critical parameter values small variations can lead to bifurcations where the change in the long-term dynamics can be dramatic. The corresponding values or the zero-, one- or multi-dimensional loci of the critical parameters define the bifurcations points, curves, or surfaces which separate the parameter space into regions characterized by similar long-term behavior.

The system (4) can be written in the generic vector form

$$\frac{d\mathbf{z}}{dt} = \mathbf{f}(\mathbf{z}; \Gamma) \quad (5)$$

Here, $\mathbf{z} \in \mathbb{R}^{n_s+1}$ is the system state, $\Gamma \in \mathbb{R}^{n_\gamma}$ the vector of operating parameters, and the source term $\mathbf{f} : \mathbb{R}^{n_s+n_\gamma+1} \rightarrow \mathbb{R}^{n_s+1}$ is a smooth vector function satisfying the Lipschitz conditions. The brute-force approach is neither efficient in probing the dynamics nor accurate in determining the bifurcation points, particularly for high-dimensional phase and parameter spaces. The aim of numerical bifurcation analysis is to compute accurately and efficiently the long-term solutions of the corresponding set of the parameter-dependent nonlinear algebraic equations

$$\mathbf{f}(\mathbf{z}; \Gamma) = 0 \quad (6)$$

defining the steady state of the system as some of the n_γ parameters are varied to compute the solution branches $\mathbf{z}(\Gamma)$.

For the sake of completeness, the basic notions and dynamic features observed in this study are summarized. For a more comprehensive discussion the reader is referred to [41]. For fixed parameter values, the phase portrait is the collection of solution trajectories of Eq. (5) in phase space, the $(n_s + 1)$ -dimensional space in which all possible system states can be represented. At given parameter values Γ^* a fixed point is the steady state \mathbf{z}^* satisfying $\mathbf{f}(\mathbf{z}^*; \Gamma^*) = 0$. At long times, the system state may also evolve on a limit cycle, a closed trajectory in phase space that describes oscillatory behavior. Together with fixed points they are the most commonly observed types of limit sets. If the qualitative structure of the phase portrait changes at $\Gamma = \Gamma^*$ then a bifurcation occurs, and $(\mathbf{z}^*; \Gamma^*)$ defines the bifurcation point. The bifurcation diagram is the plot of some function of the state variable \mathbf{z} in the limit set as a function of one or more components of the controlling parameters Γ .

The local stability of a state can be characterized by the eigenvalues and eigenvectors of the Jacobian matrix of the right hand side of (5), $\mathbf{J} = \frac{\partial \mathbf{f}}{\partial \mathbf{z}}$ [24,41]. As the solution branch Γ is followed during variation of a single parameter, the eigenvalues follow trajectories on the complex plane when the real part is plotted vs the imaginary part, and bifurcations occur when the eigenvalue acquires a zero real part. In the generic case, when a real eigenvalue crosses zero at $(\mathbf{z}_{TP}; \Gamma_{TP})$, two fixed points collide and disappear at a turning point bifurcation. When a complex pair of eigenvalues with negative real part crosses the imaginary axis at $(\mathbf{z}_{HB}; \Gamma_{HB})$, a stable state loses stability at a Hopf bifurcation point and in the generic case a limit cycle is born. It can be shown that these codimension one bifurcation points (i.e. obtained by varying a single parameter) follow curves when a second parameter is varied simultaneously which can meet at codimension-two points. These higher codimension bifurcations play the role of organizing centers of lower-order bifurcations [41]. At a cusp bifurcation point two turning point curves meet tangentially and the parameter space is divided into regions having a different number of steady states. At a Bogdanov–Takens bifurcation, the linearization at the fixed point has a pair of real zero eigenvalue and satisfies some technical non-degeneracy conditions [41]. At a double Hopf or Hopf–Hopf point the Jacobian has two pairs of purely imaginary eigenvalues.

The package AUTO-07p [25,26] is employed for the continuation and bifurcation analysis of the system of Eq. (4). In the combustion community, AUTO has been used to study the dynamics of the Belousov–Zhabotinsky reaction [42] and for hydrogen/air mixtures in PSRs [16,18]. In order to perform a comprehensive study of *n*-heptane in a PSR, AUTO-07p was coupled with the CHEMKIN library [39] so that complex reaction mechanisms can be readily accommodated. Dynamical system analysis for high hydrocarbons is less common and the recent studies have mostly focused on the effect of varying the residence time on the reactor temperature [21,19,20]; the details of the employed continuation approach were not provided.

4. Skeletal mechanism for *n*-heptane/air mixture

Entropy production analysis was recently proposed as a method for the construction of skeletal mechanisms [23]. The rate of change of the total entropy production per unit volume due to the n_r elementary reactions reads

$$\frac{dS}{dt} = R_c \sum_{k=1}^{n_r} (q_k^f - q_k^r) \ln \left(\frac{q_k^f}{q_k^r} \right) \quad (7)$$

where R_c is the ideal gas constant. The relative contribution of each reaction to the total entropy production at time t is defined as

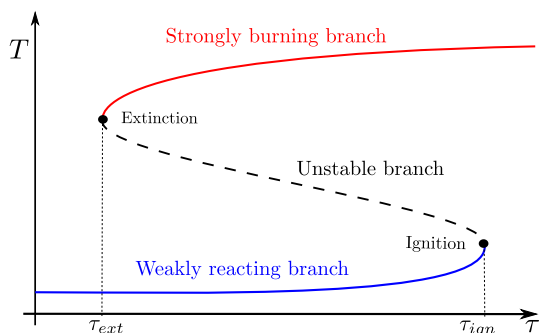


Fig. 1. Typical S-shaped bifurcation diagram of a PSR temperature with respect to the residence time.

$$r_k(t) = \left(\frac{dS}{dt} \right)^{-1} \left[R_c (q_k^f - q_k^r) \ln \left(\frac{q_k^f}{q_k^r} \right) \right] \quad (8)$$

and the most-contributing reactions can be identified as the set of reactions which contribute more than a user-specified threshold ϵ to the total entropy production

$$r_k(t) \geq \epsilon \quad (9)$$

The set of unimportant species, i.e. those not present in the most-contributing reactions, can be eliminated from the reaction mechanism. The entropy production analysis was performed for different threshold values ϵ on a solution database for *n*-heptane auto-ignition in the range of pressures $1 \leq p \leq 20$ atm, initial temperatures $650 \leq T_0 \leq 1400$ K, and equivalence ratios $0.5 \leq \phi \leq 1.5$ computed with version 2 of the detailed *n*-heptane/air mechanism (561 species and 2539 reactions) of Curran et al. [43,44], which in the following will be referred to as D561. A skeletal mechanism with 161 species and 688 reactions was constructed with $\epsilon = 0.006$ and validated for different cases in a wide range of thermodynamic conditions for auto-ignition in a constant pressure and variable volume reactor, in steady perfectly stirred reactors, and for laminar premixed flames [23].

Careful inspection of the results of time integration in a transient PSR revealed that 13 intermediate species of the skeletal mechanism that participate in important reactions appear only as reactants in irreversible reactions in the detailed mechanism. Since they cannot be produced, their concentration remains

identically zero and they can be safely removed to construct a skeletal *n*-heptane mechanism with 149 species in 669 reactions (denoted as S149); the skeletal mechanism in CHEMKIN format is provided as [supplementary material](#). Figure 2 compares the ignition delay times and laminar flame speeds. As it can be readily observed, the skeletal mechanism reproduces the results of detailed mechanism accurately. Additional details and validations can be found in [23].

The comparison of the detailed and skeletal mechanisms for the continuation with respect to the residence time for a stoichiometric mixture of *n*-heptane and air with $T_0 = 650$ K and $p = 1, 5$ and 20 atm is shown in Fig. 3. Although not marked in the figure, the skeletal mechanism is able to capture accurately not only the turning but also the Hopf bifurcation points (Table 1). It can therefore be concluded that the skeletal mechanism provides an accurate description of the kinetics and retains high fidelity to the complex non-linear dynamics of *n*-heptane oxidation in comparison to the detailed mechanism.

5. CSP analysis

The processes contributing to the dominant time scale at the bifurcation points are investigated in Section 6 via numerical tools provided by the Computational Singular Perturbation.

The system of Eq. (4) for an adiabatic PSR can be rewritten as

$$\frac{dz}{dt} = \mathbf{g}(\mathbf{z}) = \mathbf{P}(\mathbf{z}) + \mathbf{L}(\mathbf{z}) \quad (10)$$

by decomposing the right hand side in terms of the chemical source term $\mathbf{P}(\mathbf{z})$

$$\mathbf{P} = \left[\frac{W_1 \dot{\omega}_1}{\rho}, \dots, \frac{W_{n_s} \dot{\omega}_{n_s}}{\rho}, -\frac{\sum_{i=1}^{n_s} W_i \dot{\omega}_i h_i}{\rho c_p} \right]^T \quad (11)$$

and the flow term $\mathbf{L}(\mathbf{z})$

$$\mathbf{L} = \left[\frac{Y_1^0 - Y_1}{\tau}, \dots, \frac{Y_{n_s}^0 - Y_{n_s}}{\tau}, \frac{\sum_{i=1}^{n_s} Y_i^0 (h_i^0 - h_i)}{c_p \tau} \right]^T \quad (12)$$

The source term in Eq. (10) can be written as a matrix–vector product

$$\mathbf{g}(\mathbf{z}) = \mathbf{S}\mathbf{R} \quad (13)$$

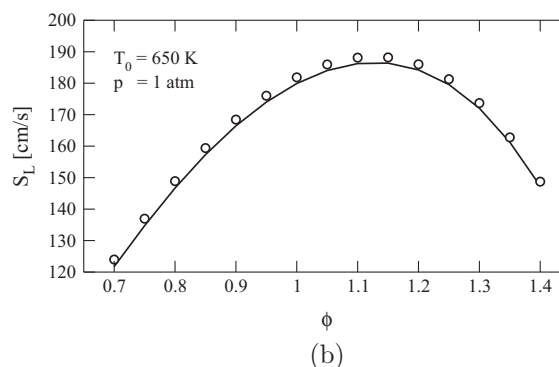
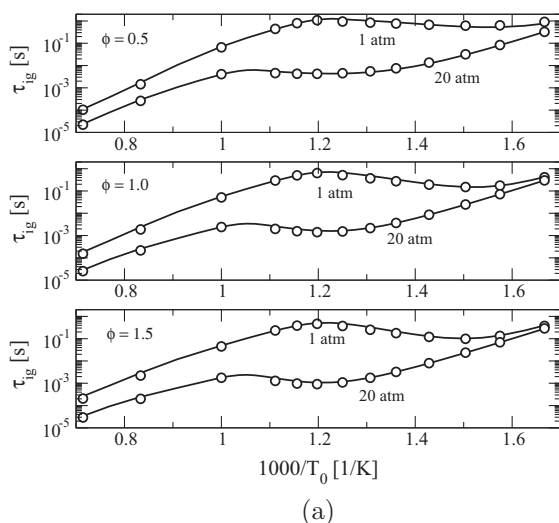


Fig. 2. Comparison of the results obtained with the skeletal (symbols) and the detailed (solid line) mechanisms for the dependence of (a) the auto-ignition delay time on the initial temperature at various pressures and (b) the laminar flame speed on equivalence ratio.

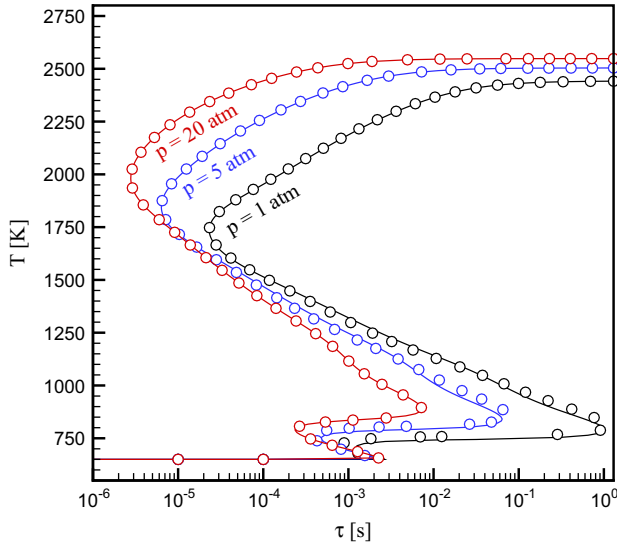


Fig. 3. Comparison of the dependence of reactor temperature on the residence time for an adiabatic PSR at $T_0 = 650$ K, $\phi = 1.0$ and various pressures using the detailed (solid lines) and skeletal (open circles) reaction mechanisms.

where \mathbf{S} is the $(n_s + 1) \times (2n_r + 1)$ -dimensional generalized stoichiometric matrix (forward and reverse reactions are treated separately)

$$\mathbf{S} = \begin{bmatrix} \frac{W_1 v_{11}}{\rho} & \dots & \frac{W_1 v_{1n_r}}{\rho} & \frac{-W_1 v_{11}}{\rho} & \dots & \frac{-W_1 v_{1n_r}}{\rho} & \frac{Y_1^0 - Y_1}{\tau} \\ \frac{W_2 v_{21}}{\rho} & \dots & \frac{W_2 v_{2n_r}}{\rho} & \frac{-W_2 v_{21}}{\rho} & \dots & \frac{-W_2 v_{2n_r}}{\rho} & \frac{Y_2^0 - Y_2}{\tau} \\ \vdots & \vdots & \vdots & \vdots & \vdots & \vdots & \vdots \\ \frac{W_{n_s} v_{n_s 1}}{\rho} & \dots & \frac{W_{n_s} v_{n_s n_r}}{\rho} & \frac{-W_{n_s} v_{n_s 1}}{\rho} & \dots & \frac{-W_{n_s} v_{n_s n_r}}{\rho} & \frac{Y_{n_s}^0 - Y_{n_s}}{\tau} \\ -\sum_{i=1}^{n_s} \frac{h_i W_i v_{i1}}{\rho c_p} & \dots & -\sum_{i=1}^{n_s} \frac{h_i W_i v_{i n_r}}{\rho c_p} & \sum_{i=1}^{n_s} \frac{h_i W_i v_{i1}}{\rho c_p} & \dots & \sum_{i=1}^{n_s} \frac{h_i W_i v_{i n_r}}{\rho c_p} & \sum_{i=1}^{n_s} \frac{(h_i^0 - h_i) Y_i^0}{c_p \tau} \end{bmatrix} \quad (14)$$

and $\mathbf{R} = [q_1^f, \dots, q_{n_r}^f, q_1^r, \dots, q_{n_r}^r, 1]^T$ is the $(2n_r + 1)$ -dimensional vector of the generalized rates of progress.

Systems enjoying time scale separation are evolving in fast and slow subspaces embedded in the phase space. A typical scenario in chemical kinetics is a spectrum of time scales, τ_i , where the first F scales are much faster than the rest and there is a large gap between the F and $F + 1$ time scales

$$\tau_1 < \dots < \tau_F \ll \tau_{F+1} < \dots < \tau_{n_s+1} \quad (15)$$

CSP [33] offers an algorithm to decompose the dynamics into iteratively refined modes, which span the fast and slow subspaces. Recasting Eq. (13) in terms of the CSP modes, one can write

$$\mathbf{g} = \mathbf{g}_{fast} + \mathbf{g}_{slow} = \sum_{i=1}^F \mathbf{a}_i^{fast} m_i^{fast} + \sum_{i=F+1}^{n_s+1} \mathbf{a}_i^{slow} m_i^{slow} \quad (16)$$

where \mathbf{a}_i is the $(n_s + 1)$ -dimensional CSP column basis vector for the i th mode with amplitude $m^i = \mathbf{b}^i \cdot \mathbf{g}$. The complementary vector space element \mathbf{b}^i is the CSP row basis vector satisfying orthogonality condition (written in Kronecker form) $\mathbf{b}^i \cdot \mathbf{a}_j = \delta_j^i$. Typically the F fastest time scales are dissipative, the corresponding CSP modes quickly become exhausted and the system state evolves on the slow subspace, which can be approximated by

$$m_{fast}^i \approx 0 \quad i = 1, \dots, F \quad (17)$$

The relaxation on the slow subspace is then governed by

$$\frac{dz}{dt} \approx \mathbf{g}_{slow} \quad (18)$$

Local information for the system time scales can be obtained from \mathbf{J}_g , the Jacobian of \mathbf{g} at the desired state. For real eigenvalues (complex pairs are treated as described in [35,45]), the CSP i th mode can be distinguished with a time scale approximated by $\tau \approx |\lambda_i|^{-1}$, the i th eigenvalue of \mathbf{J}_g [46]. The right eigenvectors \mathbf{v}_i stored columnwise define the $(n_s + 1) \times (n_s + 1)$ matrix \mathbf{V}

$$\mathbf{V} = [\mathbf{v}_1, \mathbf{v}_2, \dots, \mathbf{v}_{n_s+1}] \quad (19)$$

while the i th row of matrix \mathbf{V}^{-1} is the i th left eigenvector $\tilde{\mathbf{v}}_i$ of the Jacobian

$$\mathbf{V}^{-1} = \begin{bmatrix} \tilde{\mathbf{v}}_1^T \\ \tilde{\mathbf{v}}_2^T \\ \vdots \\ \tilde{\mathbf{v}}_{n_s+1}^T \end{bmatrix} \quad (20)$$

To leading order CSP vectors can be approximated by the right and left eigenvectors, i.e. $\mathbf{a}_i = \mathbf{v}_i$ and $\mathbf{b}^i = \tilde{\mathbf{v}}_i^T$ [46].

The decomposition approach briefly presented above, leads to the introduction of different diagnostic tools to quantify the contribution of species and reactions or other processes to the CSP mode of interest. The i th CSP mode can be characterized based on the sign of $Re(\lambda_i)$, the real part of the eigenvalue of \mathbf{J}_g . The CSP mode related to the positive or less negative eigenvalue plays the main role in limiting phenomena like ignition and extinction [19–21,31,32,47].

The contribution of process k to the amplitude of the i th CSP mode can be computed with the help of the *amplitude participation index* [33,35,21,36]

$$API_k^i = \frac{(\tilde{\mathbf{v}}_i^T \cdot \mathbf{S}_k) R^k}{\sum_{k'=1}^{2n_r+1} |(\tilde{\mathbf{v}}_i^T \cdot \mathbf{S}_{k'}) R^{k'}|} \quad (21)$$

Table 1
Comparison of the bifurcation points computed with the detailed (D561) and the skeletal (S149) mechanisms; TP₁ and HB₁ are as marked in Fig. 4 (adiabatic PSR at $T_0 = 650$ K, $\phi = 1$).

| p [atm] | TP ₁ (τ [s], T [K]) | TP ₂ (τ [s], T [K]) | TP ₃ (τ [s], T [K]) | HB ₁ (τ [s], T [K]) |
|-------------|--|--|--|--|
| <i>D561</i> | | | | |
| 1 | (2.32×10^{-5} , 1735.4) | (1.02, 790.2) | (1.22×10^{-3} , 706.5) | (1.04×10^{-2} , 741.9) |
| 5 | (6.35×10^{-6} , 1846.1) | (6.38×10^{-2} , 840.3) | (4.75×10^{-4} , 749.6) | (3.13×10^{-3} , 789.0) |
| 20 | (2.78×10^{-6} , 1981.4) | (7.24×10^{-3} , 889.0) | (2.37×10^{-4} , 789.9) | (9.21×10^{-4} , 833.8) |
| <i>S149</i> | | | | |
| 1 | (2.33×10^{-5} , 1739.2) | (1.08, 807.3) | (8.41×10^{-4} , 717.3) | (6.98×10^{-3} , 756.5) |
| 5 | (6.39×10^{-6} , 1849.5) | (7.34×10^{-2} , 859.5) | (3.76×10^{-4} , 760.1) | (2.29×10^{-3} , 803.2) |
| 20 | (2.81×10^{-6} , 1983.8) | (8.93×10^{-3} , 908.4) | (2.24×10^{-4} , 800.3) | (7.09×10^{-4} , 844.7) |

where $k = 1, \dots, n_r$ and $k = n_r + 1, \dots, 2n_r$ correspond to the contribution of the forward and reverse reaction rates and $k = 2n_r + 1$ to the contribution of flow term. The API values are normalized to $[0, 1]$ and complex conjugate pairs of modes can be transformed into a pair of real modes as described in [35,45].

The Jacobian matrix \mathbf{J}_g can be decomposed based on the contribution of the processes,

$$\mathbf{J}_g = \sum_{k=1}^{2n_r+1} \mathbf{c}_k \quad (22)$$

where the $\mathbf{c}_k = \nabla(\mathbf{S}_k R^k)$ is the $(n_s + 1) \times (n_s + 1)$ -dimensional gradient of the vector $\mathbf{S}_k R^k$. The i th eigenvalue of \mathbf{J}_g can then be written as,

$$\lambda_i = \tilde{\mathbf{v}}_i^T \cdot \mathbf{c}_1 \mathbf{v}_i + \dots + \tilde{\mathbf{v}}_i^T \cdot \mathbf{c}_{2n_r+1} \mathbf{v}_i \quad (23)$$

and the normalized contribution of process k to the value of the i th eigenvalue (i th time scale) defines the *timescale participation index* [34,48,20,46],

$$\text{TPI}_k^i = \frac{\tilde{\mathbf{v}}_i^T \cdot \mathbf{c}_k \mathbf{v}_i}{\sum_{k'=1}^{2n_r+1} |\tilde{\mathbf{v}}_i^T \cdot \mathbf{c}_{k'} \mathbf{v}_i|} \quad (24)$$

The analytic Jacobian matrix used in the CSP analysis is obtained by applying the automatic differentiation tool Taped [49] on the source code of the transient PSR, and the eigenvalues and the left and right eigenvectors of the Jacobian were computed using LAPACK routines [50]. In the following, we will only analyze the explosive mode corresponding to the leading eigenvalue, i.e. the one with positive or least negative real part, to identify the dominant process and reactions for ignition, extinction and oscillatory behavior.

In addition to the time scale analysis, entropy production, plays an important role in characterizing the reversibility of the system [51]. Chemical affinity, Gibbs free energy and entropy production are closely related [52,53]. The reactions which contribute more in the production of entropy are responsible for relaxing the system from the initial state towards the maximum entropy state (equilibrium) and can be ranked accordingly (see for example [54] for a combustion application). In this work, entropy production analysis will be applied at bifurcation points to identify the reactions which are responsible for combustion irreversibility.

6. Continuation and bifurcation analysis

In this section, the effect of the variation of the system parameters on the dynamics of n -heptane/air mixtures in adiabatic and non-adiabatic perfectly stirred reactors are investigated using AUTO-07p [26].

6.1. One parameter continuations

6.1.1. Adiabatic reactor: effect of residence time

The bifurcation diagram for the combustion of a stoichiometric mixture in an adiabatic PSR at atmospheric pressure and inlet temperature $T_0 = 700$ K displays five branches (Fig. 4(a)). In addition to the commonly observed strongly burning state, the unburned or weakly burning states and the connecting unstable branch drawn in Fig. 1, the cool flame and a short unstable branch connecting it to the extinguished reactor state are found. The cool flame behavior is associated with a small increase of the reactor temperature ($732 \leq T \leq 820$ K) and is characteristic of higher hydrocarbons displaying multi-stage ignitions and the Negative Temperature Coefficient (NTC) regime [55]. The branches are separated by the four turning points TP_i and the analysis reveals two additional Hopf bifurcation points HB_i leading to oscillatory dynamics as discussed below. Similar bifurcations are reported in [21] for a $\phi = 0.5$ mixture at $p = 10$ atm.

The first turning point at $\tau_{\text{TP}_1} = 0.0206$ ms ($T_{\text{TP}_1} = 1753.5$ K) marks the extinction limit of the strongly burning state as can be verified by time integration of the transient Eq. (4) starting from an initial condition at TP_1 and reducing the initial reactor temperature by 1 K: the response shows a fast drop of the reactor temperature to that of the inflowing mixture (Fig. 5(a)). The most contributing reactions to the total entropy production as well as the important reactions identified by time scale analysis of the CSP mode with positive eigenvalue are provided in Fig. 5(b)–(d). At TP_1 , the leading eigenvalue is zero. To avoid numerical difficulties with the infinite time scale, the CSP analysis was performed slightly to the right of the bifurcation point on the unstable branch. Although the leading eigenvalue changes rapidly around TP_1 , the ordering of the reactions and the indices were found to be insensitive to the chosen point. The APIs reveal that extinction is controlled by the competition between the flow (negative index as expected from the transition to the extinguished branch by an

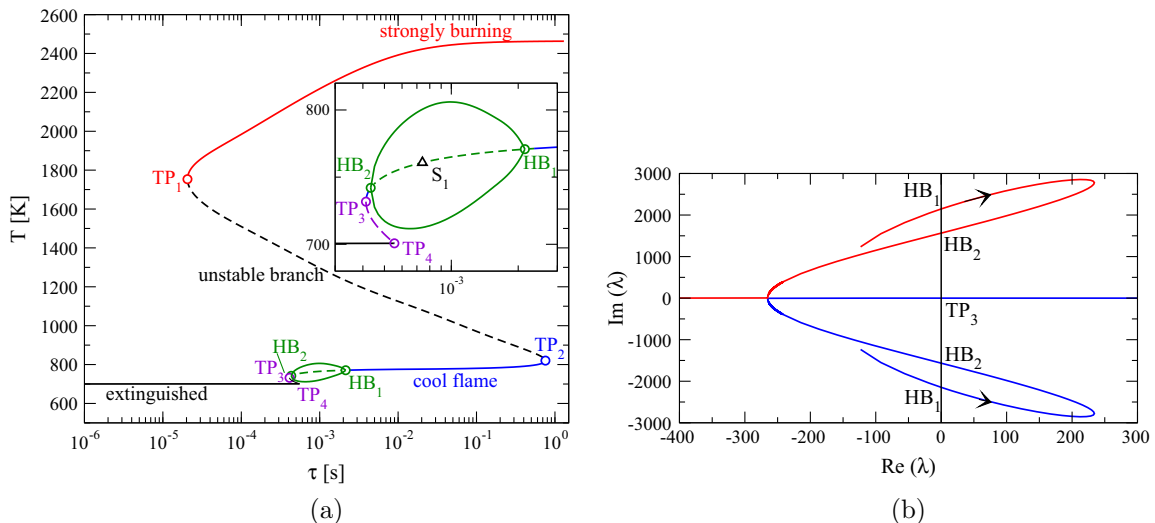


Fig. 4. (a) Reactor temperature as a function of residence time for a stoichiometric n -heptane/air mixture ($p = 1$ atm, $T_0 = 700$ K) in an adiabatic PSR. Solid (dashed) lines indicate stable (unstable) states, while the solid curves between HB_1 and HB_2 of the expanded inset show the maximum and minimum reactor temperatures during the oscillations. (b) Trajectories of the leading eigenvalues along the cool flame branch for $\tau < 6 \times 10^{-3}$ s.

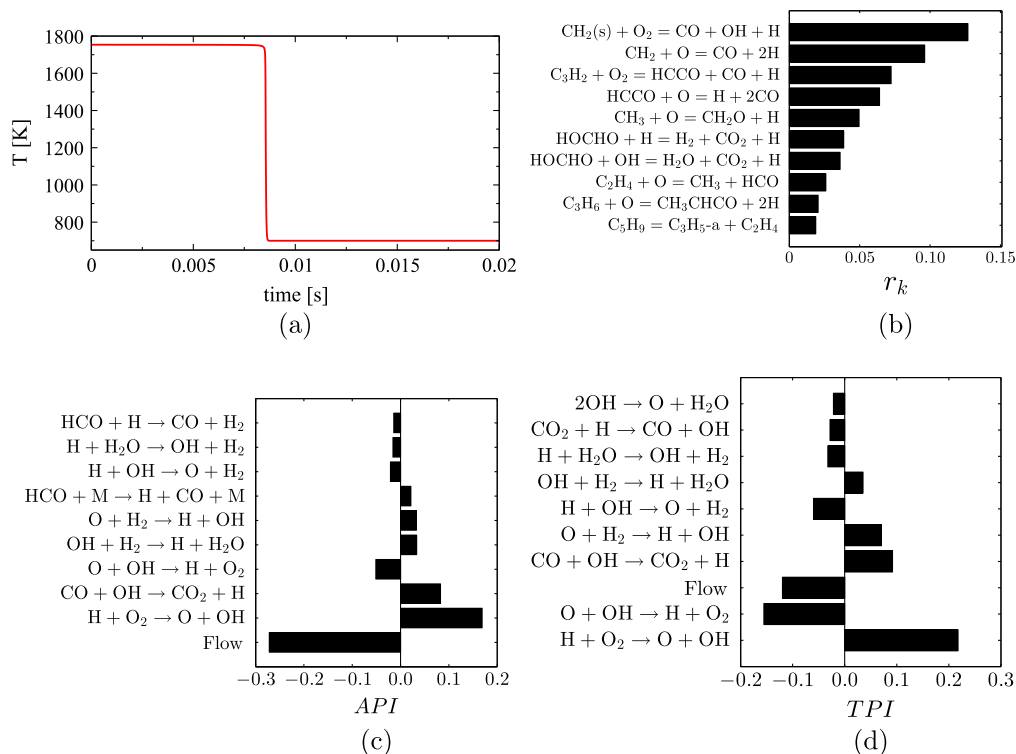


Fig. 5. Extinction of the strongly burning state at TP_1 ($T = 1753.5$ K, $\tau = 0.0206$ ms): (a) Temperature evolution in the transient PSR after reduction of the reactor temperature by 1 K, (b) Most contributing reactions in the total entropy production, (c) amplitude participation indices, (d) timescale participation indices ($p = 1$ atm, $T_0 = 700$ K).

increase in the flow rate, i.e. decrease in the residence time) and the elementary reactions responsible for the main chain branching step at high temperatures, $\text{H} + \text{O}_2 \rightarrow \text{O} + \text{OH}$, and the main heat releasing reaction, $\text{CO} + \text{OH} \rightarrow \text{CO}_2 + \text{H}$ (positive indices indicating that an increase in the rates of these reactions will favor the strongly burning state). The dominant time scale at the chosen point ($\tau_1 = 1/\lambda_1 = 6.97 \times 10^{-4}$ s) is determined by the main chain branching reaction (positively in the radical-producing direction, negatively in the reverse direction) and negatively by the cold inflow. The main heat releasing step together with the secondary chain branching step $\text{O} + \text{H}_2 \rightarrow \text{H} + \text{OH}$ have a positive contribution. Entropy production and thus irreversibility is dominated by reactions including small molecules.

The second turning point at $\tau_{TP_2} = 0.7571$ s ($T_{TP_2} = 820.3$ K) marks the ignition conditions towards the strongly burning state. Indeed, a 1 K increase of the initial reactor temperature from the conditions at TP_2 results in a jump to the strongly burning state (Fig. 6(a)). Entropy production analysis reveals that reactions responsible for the breakup of heavy molecules are most important with respect to irreversibility (Fig. 6(b)), while CSP analysis performed slightly to the left of TP_2 on the unstable branch (Figs. 6(c) and (d)) shows the clearly dominant role of the reaction $\text{H}_2\text{O}_2 + \text{M} \rightarrow 2\text{OH} + \text{M}$, the main branching step at low temperature [56], both in the amplitude and in the time scale ($\tau_1 = 6.09$ s) of the leading eigenmode. Flow has again a negative contribution. Similar findings are reported in [35,30] for autoignition of a stoichiometric *n*-heptane/air mixture in a constant volume batch reactor at 850 K and 13.5 bar.

Along the cool flame branch, the segment connecting the two supercritical Hopf bifurcation points HB_1 and HB_2 (dashed line in the inset of Fig. 4(a), with the solid lines marking the oscillation amplitude) defines the range of residence times for which the *n*-heptane cool flames exhibit oscillatory behavior. The trajectories of the complex pair of eigenvalues on the complex plain (imaginary

part plotted against the real part) as τ is decreased from $\tau = 6$ ms along the cool flame branch of Fig. 4(b) show the two crossings of the real axis at the Hopf bifurcation points HB_1 and HB_2 , their meeting at $\tau = 4.13$ ms to become real, and their subsequent trajectories along the real axis. One of them crosses to positive values at turning point τ_{TP_3} .

The time history of the state initialized at point S_1 ($\tau = 0.7412$ ms, $T = 760.84$ K, Fig. 4(a)) shows the evolution to a limit cycle with a frequency of about 240 Hz (Fig. 7(a)). At the unstable steady state S_1 , the kinetics are determined by the set of reactions shown in Fig. 7(b)–(d). Reactions containing heavy molecules are most-contributing in the total entropy production. The APIs show that the dominant reactions are the dehydrogenation of *n*-heptane by hydroxyl radicals to produce different isomers of the heptyl radical C_7H_{15} and initiate the formation of the radical pool, while the flow term has again the main negative contribution. In addition, ketohydroperoxide molecules are formed from isomerization of peroxy-alkylhydroperoxide radicals. The real part of the dominant eigenvalue at S_1 is positive. The TPI shows that the slowest timescale of the unstable state at S_1 ($\tau_1 = 4.51 \times 10^{-3}$ s) is due to the reactions $\text{CH}_2\text{O} + \text{OH} \rightarrow \text{HCO} + \text{H}_2\text{O}$ and $\text{HO}_2 + \text{OH} \rightarrow \text{H}_2\text{O}$. At this point, flow has a contribution only on API, which is positively affected by the H abstraction reactions by the hydroxyl radical. As shown in [57] for a simple glycolysis model, CSP analysis can also be used to identify the processes controlling the oscillatory behavior. For the high-dimensional *n*-heptane combustion, such a study is significantly more complicated and beyond the scope of this work.

The steady cool flame becomes stable for a narrow interval when $\tau < \tau_{HB_2}$, and eventually disappears for a shorter residence time at the third turning point TP_3 ($\tau = 0.413$ ms, $T = 731.72$ K, Fig. 4(a)). As shown in Fig. 8(a), a reactor initialized at a temperature slightly lower than T_{TP_3} evolves towards the inlet temperature; TP_3 corresponds to the first stage ignition point of

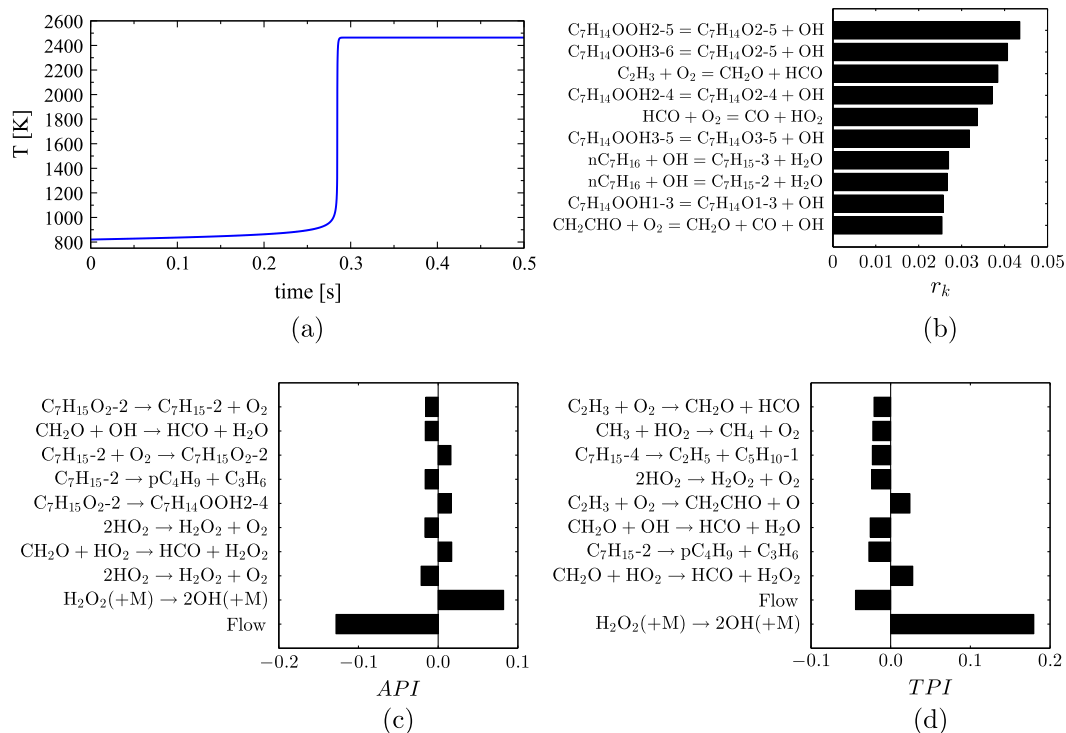


Fig. 6. Ignition of the cool flame at TP₂ ($T = 820.3 \text{ K}$, $\tau = 0.7571 \text{ s}$): (a) Temperature evolution in the transient PSR after increasing the reactor temperature by 1 K, (b) Most contributing reactions in the total entropy production, (c) amplitude participation indices, (d) timescale participation indices ($p = 1 \text{ atm}$, $T_0 = 700 \text{ K}$).

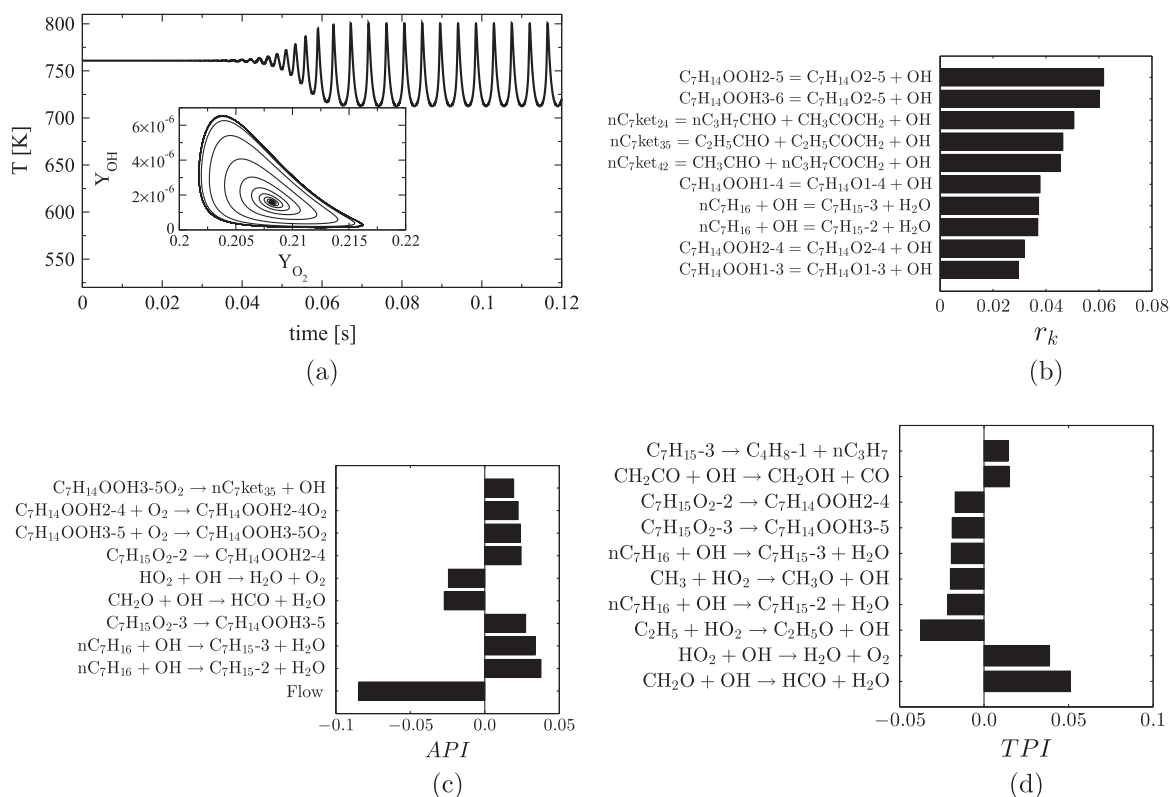


Fig. 7. Oscillatory dynamics at the sample point S₁ ($\tau = 0.7412 \text{ ms}$, $T = 760.84 \text{ K}$): (a) Temperature evolution in the transient PSR together with a projection of a sample trajectory on the (Y_{OH} , Y_{O_2}) phase plane, (b) most contributing reactions in the total entropy production, (c) amplitude participation indices, (d) timescale participation indices ($p = 1 \text{ atm}$, $T_0 = 700 \text{ K}$).

n-heptane/air mixtures. The explosive mode amplitude is very sensitive to the residence time, while chemistry is dominated by

isomerization (internal H-atom abstraction) and dehydrogenation reactions via OH and O₂ (Fig. 8(c) and (d)). For low temperature

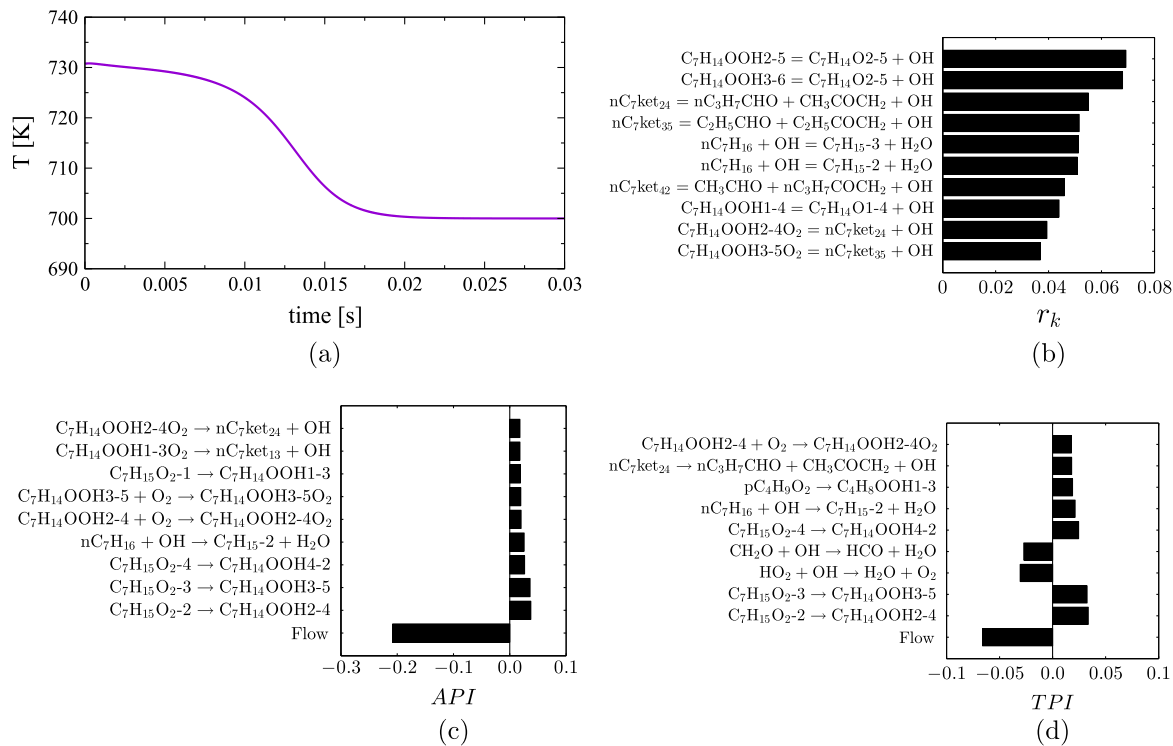


Fig. 8. Cool flame extinction limit TP_3 ($T = 731.72$ K, $\tau = 0.413$ ms): (a) Temperature evolution in the transient PSR after decreasing the reactor temperature by 1 K, (b) most contributing reactions in the total entropy production, (c) amplitude participation indices, (d) time scale participation indices ($p = 1$ atm, $T_0 = 700$ K).

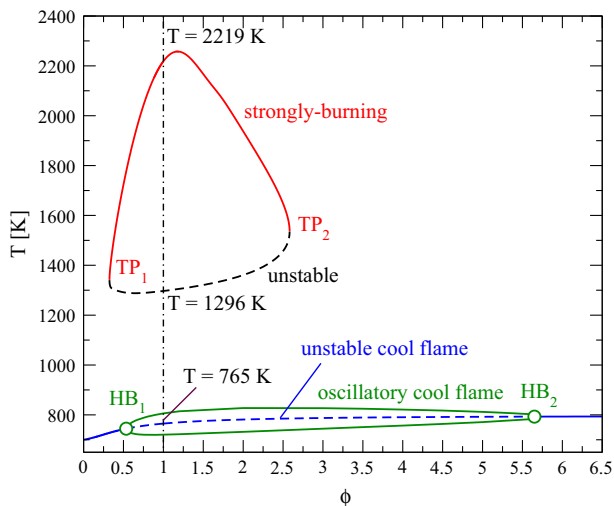


Fig. 9. Dependence of the reactor temperature on equivalence ratio for the adiabatic PSR at $p = 1$ atm, $T_0 = 700$ K and $\tau = 1$ ms. Solid (dashed) lines indicate stable (unstable) steady states.

ignition of *n*-heptane, the same class of reactions are found to dominate the oxidation path in [29]. All along the cool flame branch, entropy is produced by reactions involving large molecules.

Finally, another unstable branch connects the cool flame to the extinguished reactor state at the fourth turning point TP_4 at $\tau = 0.56$ ms and $T = 700.0013$ K (expanded inset in Fig. 4(a)).

6.1.2. Adiabatic reactor: effect of equivalence ratio

According to Fig. 4(a), the stoichiometric mixture in a PSR with $\tau = 1$ ms can support three steady states with reactor

temperatures equal to 2219 K (stable, strongly burning), 1296 K (unstable intermediate state) and 765 K (unstable cool flame), and one stable oscillatory state around the cool flame. The effect of the variation of ϕ on the reactor temperature at fixed $\tau = 1$ ms is shown in Fig. 9. Three branches can again be seen, but the bifurcation diagram in this case displays an isola containing the stable strongly burning state and the unstable branch within the flammability range $0.325 \leq \phi \leq 2.582$, which is not connected to the cool flame branch. The maximum temperature of the strongly burning state occurs slightly on the rich side of the fuel equivalence ratio ϕ , as expected from the off-stoichiometric peak of the adiabatic flame temperature for hydrocarbon/air mixtures [7]. The isola is clearly separated from the cool flame branch which extends over the whole range of ϕ with temperatures $T_0 \leq T \leq 793.8$ K. Since for $\phi \geq 2.582$ the cool flame is the only steady reactor state, its kinetics can be isolated and effectively studied.

The changes in the bifurcation diagram that lead to the formation of the isola as the residence time is varied are shown in Fig. 10. The isola exist for $\tau \leq 0.1$ s (Fig. 10(c)), but disappear for $\tau = 0.2$ s (Fig. 10(b)) after the unstable and the cool flame branch merge at some intermediate residence time. For $\tau = 1$ s the bistability region shrinks to $0.172 \leq \phi \leq 0.775$, and at long enough residence times the T - ϕ diagram will assume the familiar shape of the adiabatic flame temperature vs. equivalence ratio curve [7]. At low residence times the size of the isola, and with it the flammability range, decrease and at sufficiently low τ the cool flame branch disappears (reactor temperature equal to T_0 , Fig. 10(f)).

6.1.3. Effect of heat loss

The dependence of the reactor temperature on heat loss for the stoichiometric mixture at atmospheric pressure and for $\tau = 1$ s and $T_0 = 700$ K is depicted in Fig. 11. At these conditions, the adiabatic ($\dot{Q}_{loss} = 0$) reactor can only operate at the strongly burning state ($T = 2463$ K), but as the heat loss increases the reactor temperature decreases and hysteretic behavior is observed. Two turning

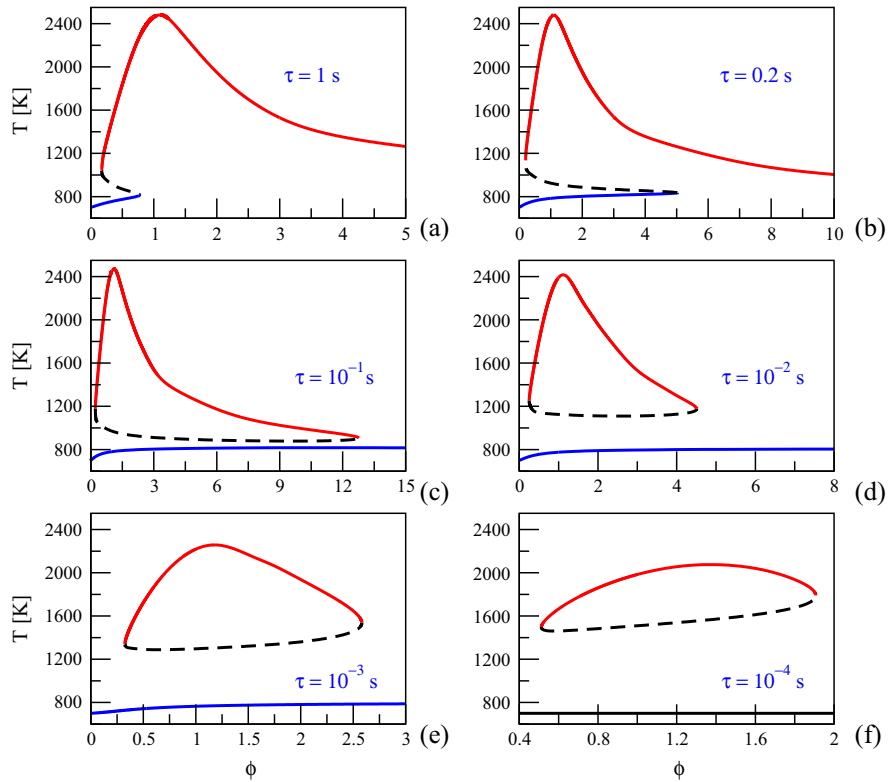


Fig. 10. The dependence of temperature reactor on the equivalence ratio in the adiabatic PSR with $T_0 = 700$ K and $p = 1$ atm at (a) $\tau = 1$ s, (b) $\tau = 0.2$ s, (c) $\tau = 10^{-1}$ s, (d) $\tau = 10^{-2}$ s, (e) $\tau = 10^{-3}$ s, (f) $\tau = 10^{-4}$ s.

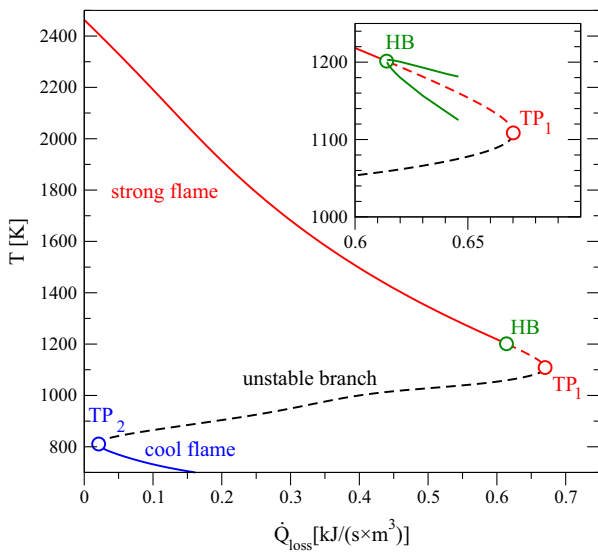


Fig. 11. The dependence of temperature reactor on heat loss in the PSR ($\phi = 1.0, T_0 = 700$ K, $p = 1$ atm and $\tau = 1$ s). Solid (dashed) lines indicate stable (unstable) branches.

points mark the conditions where no strongly burning state ($TP_1, \dot{Q}_{loss} = 0.67$ kJ/s m^3) or cool flame ($TP_2, \dot{Q}_{loss} = 0.02$ kJ/s m^3) can be supported in the reactor, while the existence of the Hopf bifurcation point HB ($\dot{Q}_{loss} = 0.614$ kJ/s $m^3, T = 1201.3$ K) before TP_1 indicates that the strongly-burning flame extinguishes dynamically. The solid curves emanating from HB in the inset of Fig. 11 and marking the oscillation amplitude show that the limit cycle

exists for $\dot{Q}_{loss_{HB}} \leq \dot{Q}_{loss} < 0.6459$ kJ/s m^3 and disappears suddenly, probably in a global bifurcation involving the limit cycle and the saddle point which is difficult to locate in such a high-dimensional phase space.

The long-term behavior along the unstable branch connecting the HB to the TP_1 point in Fig. 11 becomes very sensitive to the initial condition. Figure 12 shows that for $\dot{Q}_{loss} = 0.646$ kJ/(s m^3) starting from two initial conditions taken along the dashed line connecting HB to TP_1 in Fig. 11 and slightly perturbing the reactor temperature, either a multi-period limit cycle ($T = 1140$ K, Fig. 12(a)) or extinction ($T = 1137.8$ K, Fig. 12(b)) can be observed.

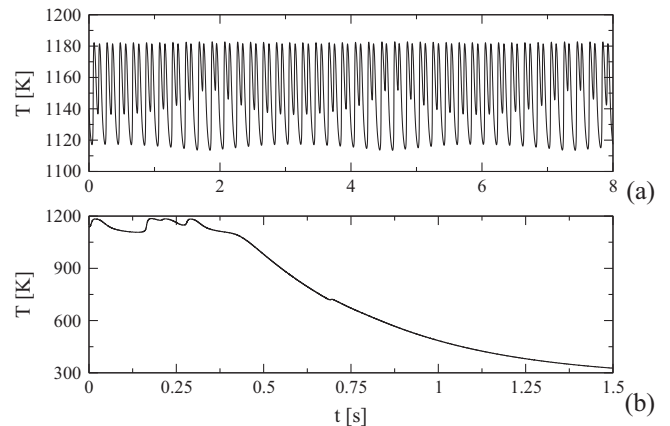


Fig. 12. Temporal evolution of the reactor temperature for non-adiabatic PSR with $\dot{Q}_{loss} = 0.646$ kJ/(s m^3) ($p = 1$ atm, $T_0 = 700$ K, $\phi = 1, \tau = 1$ s). Different initial conditions results in (a) multi-period transient solution for initial $T = 1140$ K or (b) dynamic extinction for $T = 1137.8$ K.

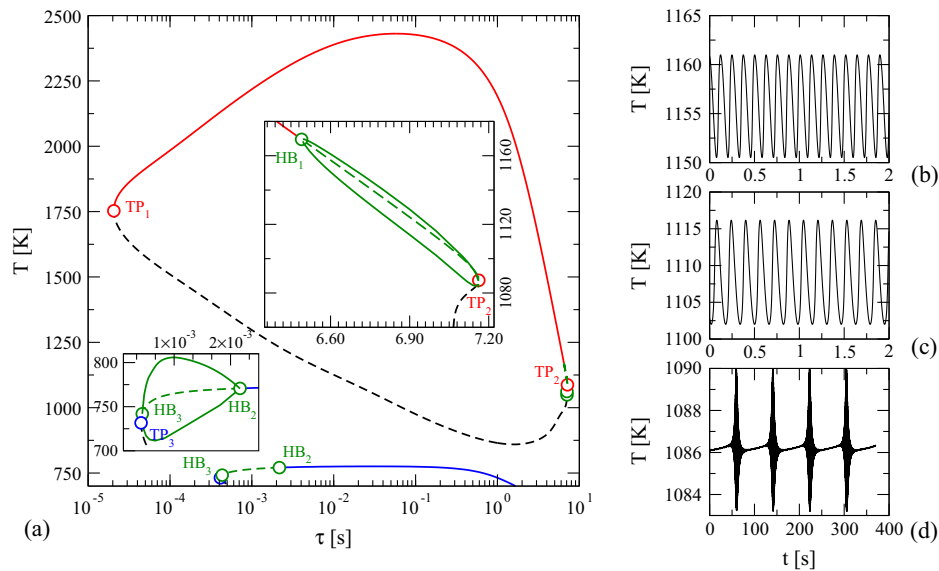


Fig. 13. (a) Dependence of reactor temperature on residence time for non-adiabatic PSR with $\dot{Q}_{\text{loss}} = 0.1 \text{ kJ}/(\text{s m}^3)$ ($p = 1 \text{ atm}$, $T_0 = 700 \text{ K}$, $\phi = 1$); time history of reactor temperature for (b) $\tau = 6.6 \text{ s}$, (c) $\tau = 7.0$, (d) $\tau = 7.1605$. Solid (dashed) lines indicate stable (unstable) branches.

Isolas also exist in the non-adiabatic case as shown in Fig. 13 for $\dot{Q}_{\text{loss}} = 0.1 \frac{\text{kJ}}{\text{s m}^3}$. Hopf bifurcation points are found along the unstable (inset inside the isola) and the cool flame branch (inset at lower left corner). The oscillations for $\tau_{\text{HB}_1} \leq \tau \leq \tau_{\text{TP}_2}$ have amplitudes of about 10 K and the period increases with increasing residence time (Fig. 13(b) and (c), periods of 0.12 and 0.17 s, respectively). Close to the turning point, the reactor operation is characterized by long intervals (close to 70 s) of slow increase of the temperature followed by oscillations with a period of approximately 0.3 s (Fig. 13(d)), indicating that the limit cycle disappears at a global bifurcation involving the nearby saddle point [41].

6.2. Multi-parameter continuation

Continuation of the turning and Hopf bifurcation points while simultaneously varying two parameters results in bifurcation curves which delineate regions on parameter planes with similar long-term dynamics. For the 150-dimensional system considered here, the two-parameter continuation with AUTO-07p requires careful choice of the numerical parameters and the bifurcation diagram had to be constructed in a piecewise manner.

6.2.1. Adiabatic reactor: effect of residence time and inlet mixture temperature

We now consider the effect of the simultaneous variation of the residence time and the inlet temperature on the four turning and the two Hopf bifurcation points of Fig. 4(a). The results are plotted in Fig. 14(a) together with one-parameter diagrams at selected T_0 (Fig. 14(b)–(e); Fig. 4 should also be consulted for the notation). The turning point branches for the cool flame ignition (TPB_2) and the strongly-burning state extinction (TPB_1) meet tangentially at the cusp point CP_1 for an impractically short residence time $(\tau, T_0) = (1.9 \times 10^{-6} \text{ s}, 1805.9 \text{ K})$, and the parameter ranges between them define the regime of multistability. To the left of the TPB_1 bifurcation curve and for inlet temperature lower than the T_{CP_1} the residence time is so low that the reactor cannot be ignited at any inlet mixture temperature. Similarly, the turning point branches for the cool (TPB_3) and the extinguished reactor (TPB_4) states meet tangentially at the second cusp point CP_2 ($\tau = 2.3 \times 10^{-4} \text{ s}$ and $T_0 = 746.5 \text{ K}$), and the parameter range

between them defines the conditions for the coexistence of the two states.

For inlet temperatures higher than $T_{\text{CP}_1} = 1805.9 \text{ K}$, the reactor can only operate at the strongly-burning state, irrespective of the residence time (Fig. 14(e)). In the range of parameters between the bifurcation curves TPB_1 and TPB_2 and the two horizontal dashed lines passing through the CP_1 and CP_2 , two steady (weakly and strongly burning states) and one unstable steady state will be observed (Fig. 14(d)).

In the range between TPB_1 and TPB_2 and below the lower dashed line, the dynamics become more complex, involving up to seven possible limit sets: three steady and stable (unreacted mixture, cool flame and strongly burning state), three unstable steady states, and oscillatory cool flames. At inlet temperature $T_0 = 550 \text{ K}$, the lower limit for which the detailed mechanism is valid [43], one Hopf bifurcation point always exists for a residence time between the second (TPB_2) and the third (TPB_3) turning points (i.e., along the cool flame branch), as it can be seen in Fig. 14(b) for $T_0 = 600 \text{ K}$. It turns out that the second Hopf point emerges from the saddle-node TPB_3 locus at $\tau = 0.4898 \text{ s}$, $T_0 = 687.58 \text{ K}$. The HBB and TPB_3 curves meet tangentially at a Bogdanov–Takens (BT) bifurcation point of codimension two where the steady state has a double-zero eigenvalue [41]. As the value of inlet temperature is further increased, the turning point and the second Hopf point, move apart and two Hopf points begin to move closer together until finally HB_1 and HB_2 coalesce at the double Hopf bifurcation point $(\tau, T_0) = (7 \times 10^{-4} \text{ s}, 719.1 \text{ K})$, another bifurcation point of codimension two, where two pairs of complex conjugate eigenvalues change their signs simultaneously at a double Hopf bifurcation point. For $719.1 < T_0 < T_{\text{CP}_2} \text{ K}$, the whole cool flame branch is steady, as can be seen in Fig. 14(c).

As mentioned, high codimension points act as organizing centers for the dynamics (see [41] for the details on the expected behavior around such points). However, for high-dimensional systems like the one considered here it is difficult to show the expected behavior, which includes global bifurcations. Figure 15(a) shows only the transient behavior of a PSR initialized at a residence time slightly lower than BT. The reactor state starts to oscillate with increasing amplitude. Due to the low residence time compared to the BT point, the cool flame cannot sustain itself, it extinguishes suddenly and the reactor temperature returns to the inlet value.

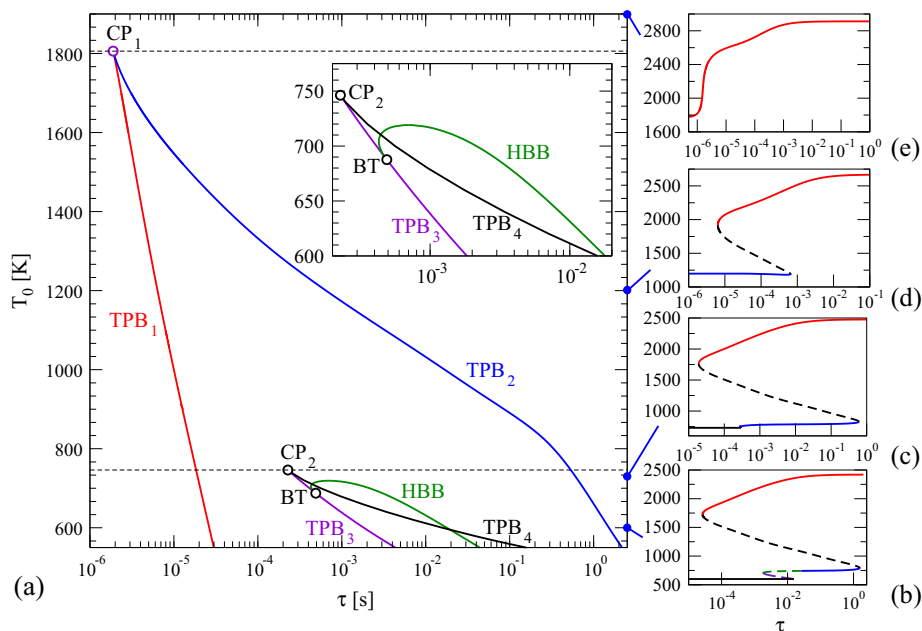


Fig. 14. (a) Two-parameter (T_0 - τ) continuation of the turning and Hopf bifurcation points of the adiabatic PSR at $p = 1$ atm and $\phi = 1$; one-parameter bifurcation diagrams (b) for $T_0 = 600$ K, (c) for $T_0 = 730$ K, (d) for $T_0 = 1200$ K, (e) for $T_0 = 1900$ K. Colors are the same as in Fig. 4(a). (For interpretation of the references to color in this figure legend, the reader is referred to the web version of this article.)

The entropy production and the CSP analysis of the mode with positive eigenvalue at the conditions of the BT point are provided in Fig. 15(b)–(d).

Some of the dynamics mentioned above occurs in narrow ranges of inlet temperatures and sometimes for very short residence times and would therefore be difficult to observe experimentally. Nevertheless, two-parameter diagrams like Fig. 14 provide invaluable information for understanding the combustion dynamics and guiding experiments in PSRs to parameter regions where the kinetics at different regimes can be effectively probed. Continuation with respect to additional parameters can help to identify parameter ranges that are more amenable to experimental investigation.

6.2.2. Adiabatic reactor: effect of pressure and equivalence ratio on the τ - T_0 bifurcation diagram

The effect of pressure and equivalence ratio on the τ - T_0 bifurcation diagram can be studied by computing the curves for different values of p and ϕ .

At higher pressure the observed bifurcations do not change, but the branches of the critical curves shift to lower residence times rendering the strongly burning state more dominant (Fig. 16(a)). The range of inlet temperatures leading to cool flame oscillations widens, but the reduction in the range of τ make their experimental investigation more difficult. The inlet composition is found to have only a minor effect on the dynamics for $\phi = 0.8, 1.0$, and 1.2 (Fig. 16(b)). Figure 16 can be considered as a projection of the three-parameter bifurcation diagram on the two-parameter space τ - T_0 . By repeating the analysis for different pressures or equivalence ratios, three-parameter diagrams can be constructed.

7. Conclusions

The complex dynamics and bifurcations of high hydrocarbons like *n*-heptane in perfectly stirred reactors were systematically investigated using a combination of time integration of the transient PSR equations and single- and multi-parameter continuation and stability analysis with AUTO-07p [26]. The study was carried

out with a skeletal mechanism with 149 species and 669 elementary reactions constructed by applying the recently proposed entropy production analysis method [23] on the detailed LLNL2 scheme [44] (561 species and 2539 reactions). Ignition delay time and flame speed over an extended range of conditions and the bifurcation points in the PSR computed with the skeletal mechanism are in very good agreement with the results computed with the detailed mechanism.

The reactor stability was investigated with respect to the residence time τ , inlet temperature T_0 , pressure p , inlet mixture equivalence ratio ϕ and heat loss \dot{Q}_{loss} . Multiple turning and Hopf bifurcation points were found in the continuation with respect to τ defining the bifurcation values and showing that up to six limit sets can coexist for the same operating conditions, both physically-realizable (steady and stable: extinguished reactor, cool flames and strongly burning state, or unsteady: cool flame oscillations) as well as unphysical (unstable steady states along the branches connecting either the turning points defining the conditions for ignition and extinction or Hopf bifurcation point leading to the oscillatory dynamics). The kinetics at the bifurcation points were analyzed with the help of the time-scale and amplitude participation indices of Computational Singular Perturbation to identify the important reactions for the explosive mode corresponding to the eigenvalue with positive or least negative real part and entropy production analysis which points to the reactions contributing most to irreversibility. Continuation with respect to equivalence ratio revealed isolas, and their appearance was studied by varying the residence time. With respect to heat loss, a Z-shaped curve was obtained, and the extinction of the strongly burning reactor was found to be dynamic (oscillatory extinction). Time integration indicated that global bifurcations also play an important role in the dynamics.

Two-parameter continuation with respect to τ and T_0 revealed the range of conditions of the different steady and oscillatory states. Codimension-two bifurcation point (cusp, Bogdanov-Takens and double Hopf) were found, but the high-dimensionality of the system complicates their detailed investigation. The effect of pressure and equivalence ratio on the two-parameter diagram was also

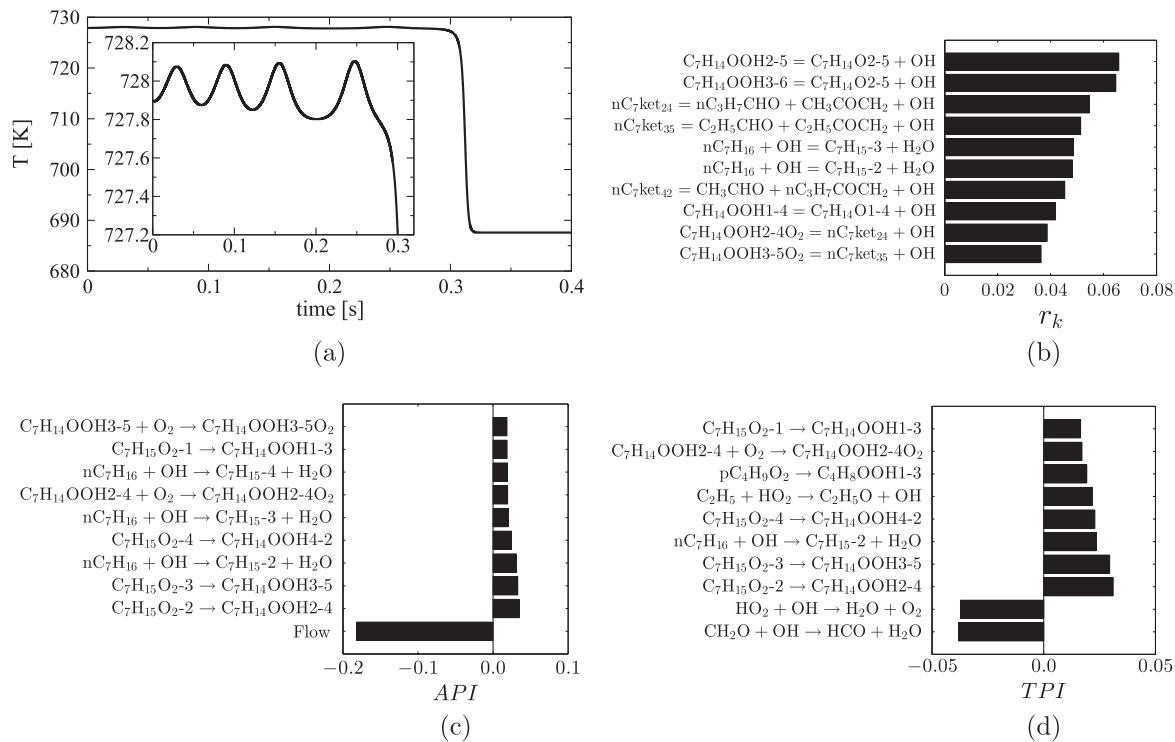


Fig. 15. The analysis of Bogdanov-Takens bifurcation point, BT ($T_0 = 687.58$ K, $T = 727.89$ K, $\tau = 0.4898$ ms): (a) Temperature evolution in the transient PSR after small perturbation in reactor temperature, (b) Most contributing reactions in the total entropy production, (c) Amplitude participation indices, (d) Time scale participation indices ($p = 1$ atm and $\phi = 1$).

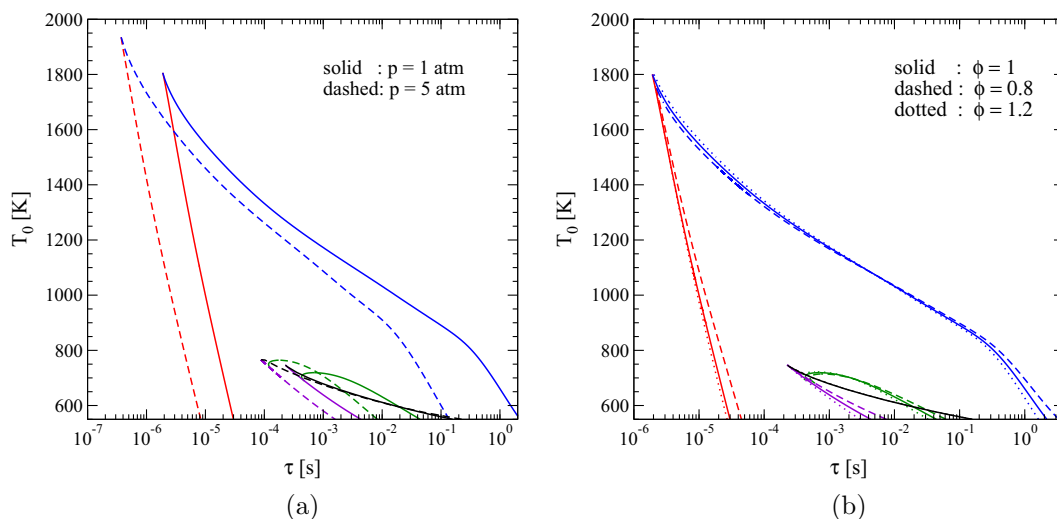


Fig. 16. Effect of (a) pressure and (b) equivalence ratio on the τ - T_0 two-parameter continuation diagrams (adiabatic PSR working at stoichiometric conditions).

studied. Increasing pressure for a stoichiometric mixture in an adiabatic PSR was found to shift the critical curves to lower residence time, but the bifurcations between different states was unaffected. Equivalence ratio variations in an atmospheric pressure adiabatic PSR have only a minor effect.

To the best of the authors' knowledge this is the first comprehensive and systematic study of the combustion dynamics of a high hydrocarbon in perfectly stirred reactors. However, the complexity resulting from both the high dimensionality of the dynamical system and the large number of parameters hinder the exploration of all possible long-term behaviors. A lot remains to be done, particularly in terms of exploring different combinations

of parameters, locating and tracking global bifurcations, and analyzing the wealth of the generated information to probe and understand the reaction kinetics determining the critical conditions.

The numerically predicted ranges of different dynamics can guide experimental investigations to interesting conditions, which will provide data for the validation or iterative refinement of detailed reaction mechanisms.

Acknowledgments

Financial support of the Swiss National Science Foundation under Project Number 137771 is gratefully acknowledged. I.V.K.

was supported by European Research Council (ERC) Advanced Grant 291094-ELBM. M.K. would like to thank Dr. Andrea Brambilla for his help with CSP analysis and AUTO.

Appendix A. Supplementary material

Supplementary data associated with this article can be found, in the online version, at <http://dx.doi.org/10.1016/j.combustflame.2015.05.002>.

References

- [1] O. Herbinet, G. Dayma, in: F. Battin-Leclerc, J. Simmie, E. Blurock (Eds.), *Cleaner Combustion, Green Energy and Technology*, Springer, 2013, pp. 183–210.
- [2] O. Bilous, N.R. Amundson, *AIChE J.* 1 (1955) 513–521.
- [3] R. Aris, N.R. Amundson, *Chem. Eng. Sci.* 7 (3) (1958) 121–131.
- [4] A. Uppal, W.H. Ray, A.B. Poore, *Chem. Eng. Sci.* 29 (1974) 967–985.
- [5] W. Farr, R. Aris, *Chem. Eng. Sci.* 41 (1986) 1385–1402.
- [6] P. Gray, S.K. Scott, *Chemical Oscillations and Instabilities*, Springer, 1996.
- [7] C.K. Law, *Combustion Physics*, Cambridge University Press, 2006.
- [8] A.B. Poore, *Arch. Ration. Mech. Anal.* 52 (1973) 358–388.
- [9] V. Balakotaiah, D. Luss, *Chem. Eng. Sci.* 37 (1982) 1611–1623.
- [10] H.S. Sidhu, M.I. Nelson, G.N. Mercer, R.O. Weber, *J. Math. Chem.* 28 (2000) 353–375.
- [11] R.B. Warden, R. Aris, N.R. Amundson, *Chem. Eng. Sci.* 19 (1964) 149–172.
- [12] F. Strozzi, J. Zaldivar, *Chem. Eng. Sci.* 49 (1994) 2681–2688.
- [13] J. Alvarez, J. Alvarez, E. González, *Chem. Eng. Sci.* 44 (1989) 1147–1160.
- [14] J. Griffiths, S. Scott, *Prog. Energy Combust. Sci.* 13 (1987) 161–197.
- [15] S. Sarathy, C. Westbrook, M. Mehl, W.J. Pitz, C. Togbe, P. Dagaut, H. Wang, M. Oehlschlaeger, U. Niemann, K. Seshadri, et al., *Combust. Flame* 158 (2011) 2338–2357.
- [16] S. Kalamatianos, D.G. Vlachos, *Combust. Sci. Technol.* 109 (1995) 347–371.
- [17] S. Kalamatianos, Y.K. Park, D.G. Vlachos, *Combust. Flame* 112 (1998) 45–61.
- [18] R.J. Olsen, D.G. Vlachos, *J. Phys. Chem. A* 103 (1999) 7990–7999.
- [19] R. Shan, T. Lu, *Combust. Flame* 159 (2012) 2069–2076.
- [20] R. Shan, T. Lu, *Combust. Flame* 161 (2014) 1716–1723.
- [21] R. Shan, C. Yoo, J. Chen, T. Lu, *Combust. Flame* 159 (2012) 3119–3127.
- [22] T. Lu, C.K. Law, *Prog. Energy Combust. Sci.* 35 (2009) 192–215.
- [23] M. Kooshkbaghi, C.E. Frouzakis, K. Boulouchos, I.V. Karlin, *Combust. Flame* 161 (2014) 1507–1515.
- [24] H. Keller, *Lectures on Numerical Methods in Bifurcation Problems*, Springer, 1987.
- [25] E.J. Doedel, *Congr. Numer.* 30 (1981) 265–284.
- [26] E. Doedel, B. Oldeman, *AUTO-07P: Continuation and Bifurcation Software for Ordinary Differential Equations*, Concordia University, Montreal, Canada, 2009.
- [27] D.A. Goussis, U.A. Maas, *Model Reduction for Combustion Chemistry, Fluid Mechanics and Its Applications*, vol. 95, Springer, Netherlands, 2011.
- [28] M. Valorani, F. Creta, D.A. Goussis, J.C. Lee, H.N. Najm, *Combust. Flame* 146 (2006) 29–51.
- [29] J. Prager, H.N. Najm, M. Valorani, D.A. Goussis, *Proc. Combust. Inst.* 32 (2009) 509–517.
- [30] D. Diamantis, D. Kyritsis, D. Goussis, in: *Second International Workshop on: Model Reduction in Reacting Flows*, pp. 49–52.
- [31] M. Valorani, H.N. Najm, D.A. Goussis, *Combust. Flame* 134 (2003) 35–53.
- [32] T. Lu, C.S. Yoo, J.H. Chen, C.K. Law, *J. Fluid Mech.* 652 (2010) 45–64.
- [33] S. Lam, D. Goussis, *Int. J. Chem. Kinet.* 26 (1994) 461–486.
- [34] D. Goussis, G. Skevis, *Comput. Fluid Solid Mech.* (2005) 650–653.
- [35] A. Kazakov, M. Chaos, Z. Zhao, F.L. Dryer, *J. Phys. Chem. A* 110 (2006) 7003–7009.
- [36] S. Gupta, H.G. Im, M. Valorani, *Proc. Combust. Inst.* 34 (2013) 1125–1133.
- [37] W. Liu, C.K. Law, T. Lu, *Int. J. Chem. Kinet.* 41 (2009) 764–776.
- [38] P.N. Brown, G.D. Byrne, A.C. Hindmarsh, *SIAM J. Sci. Stat. Comput.* 10 (1989) 1038–1051.
- [39] R.J. Kee, F.M. Rupley, E. Meeks, J.A. Miller, *CHEMKIN-III: A FORTRAN Chemical Kinetics Package for the Analysis of Gas-phase Chemical and Plasma Kinetics*, Sandia National Laboratories, Livermore, CA, 1996.
- [40] H. Meijer, F. Dercole, B. Oldeman, in: R. Meyers (Ed.), *Encyclopedia of Complexity and Systems Science*, vol. 14, Springer, 2009, pp. 6329–6352.
- [41] Y.A. Kuznetsov, *Elements of Applied Bifurcation Theory*, Springer, 1998.
- [42] R.J. Olsen, I.R. Epstein, *J. Chem. Phys.* 94 (1991) 3083.
- [43] H.J. Curran, P. Gaffuri, W.J. Pitz, C.K. Westbrook, *Combust. Flame* 114 (1998) 149–177.
- [44] https://www-pls.llnl.gov?url=science_and_technology-chemistry-combustion-nc7h16, 1998.
- [45] T. Lu, Y. Ju, C.K. Law, *Combust. Flame* 126 (2001) 1445–1455.
- [46] D.J. Diamantis, D.C. Kyritsis, D.A. Goussis, *Proc. Combust. Inst.* 35 (2015) 267–274.
- [47] Z. Luo, C.S. Yoo, E.S. Richardson, J.H. Chen, C.K. Law, T. Lu, *Combust. Flame* 159 (2012) 265–274.
- [48] D.A. Goussis, H.N. Najm, *Multiscale Model Simul.* 5 (2006) 1297–1332.
- [49] L. Hascoët, V. Pascual, *ACM Trans. Math. Soft.* 39 (2013).
- [50] E. Anderson, Z. Bai, C. Bischof, S. Blackford, J. Demmel, J. Dongarra, J. Du Croz, A. Greenbaum, S. Hammarling, A. McKenney, D. Sorensen, *LAPACK Users' Guide*, third ed., Society for Industrial and Applied Mathematics, Philadelphia, PA, 1999.
- [51] R. Tolman, P. Fine, *Rev. Mod. Phys.* 20 (1948) 51–77.
- [52] I. Prigogine, *Introduction to Thermodynamics of Irreversible Processes*, vol. 1, Interscience, New York, 1967.
- [53] T. de Donder, P. Van Rysselberghe, *Thermodynamic Theory of Affinity*, vol. 1, Stanford university press, 1936.
- [54] W. Dunbar, N. Lior, *Combust. Sci. Technol.* 103 (1994) 41–61.
- [55] I. Glassman, R. Yetter, *Combustion*, fourth ed., Academic Press, 2008.
- [56] C. Westbrook, *Proc. Combust. Inst.* 28 (2000) 1563–1577.
- [57] P. Kourdis, D. Goussis, *Math. Biosci.* 243 (2013) 190–214.